Cell and Tissue Research (2019) 378:341 358
https://doi.org/10.1007/s00441-019-03055-1

REGULAR ARTICLE

Placental cell death patterns exhibit differences throughout gestation in two strains of laboratory mice

Jacqui Detmar[1,2,3] · Isidora Rovic[1,4] · Jocelyn Ray[1,4] · Isabella Caniggia[1,2,4,5] · Andrea Jurisicova[1,4,5,6]

Received: 20 December 2018 / Accepted: 28 May 2019 / Published online: 21 June 2019

Abstract

Cell death is an essential physiological process required for the proper development and function of the human placenta. Although the mouse is a commonly used animal model for development studies, little is known about the extent and distribution of cell death in the mouse placenta throughout development and its physiological relevance. In the present study, we report the results of a systematic and quantitative assessment of cell death patterns in the placentae of two strains of laboratory mice commonly used for developmental studies—ICR and C57Bl/6. TUNEL staining revealed that ICR and C57Bl/6 placentae exhibited similar cell death patterns to those reported in human placentae during pregnancy, with comparatively infrequent death observed during early gestation, which increased and became more organized towards term. Interestingly, when comparing strain differences, increased cell death was observed in almost all regions of the inbred C57Bl/6 placentae compared to the outbred ICR strain. Finally, since Bcl-2 ovarian killer (Bok) has been reported to be a key player in human placental cell death, we examined its expression in murine placentae throughout gestation. Bok protein expression was observed in all placental regions and increased towards term in both strains. The results of this study indicate that although strain-specific differences in placental cell death exist, the overall rates and patterns of cell death during murine placentation parallel those previously described in humans. Thus, the murine placenta is a useful model to investigate molecular pathways involved in cell death signaling during human placentation.

Keywords Cell death · Murine placenta · TUNEL · Caspase-3 · Bok

Introduction

Programmed cell death (PCD)—a cell-intrinsic suicide pathway conserved in nearly all eukaryotes—is an essential feature of a number of important biological processes (Fuchs and Steller 2011). Classical, "clean" PCD is executed via activation of the apoptotic cascade; however, cells do not always take this route and may instead undergo autophagy, necroptosis, mitotic catastrophe, or may display combined features of several types of cell death (Kroemer et al. 2009). These modes of cell death have long been recognized as crucial events that regulate the morphogenesis of tissues and organs during embryogenesis. Moreover, alterations in cell death pathways have been shown to cause serious developmental abnormalities. In humans, pathological complications of pregnancy involving the placenta, such as preeclampsia (PE), intrauterine growth restriction (IUGR), spontaneous abortions, hydatidiform moles and choriocarcinoma, have been associated with abnormal patterns and regulation of cell death (Jurisicova et al. 2005; Soleymanlou et al. 2005; Sharp et al. 2010; Gong and Kim 2014; Bailey et al. 2017; Nadhan et al. 2017). Thus, well-regulated or controlled cell death is necessary for the normal development of all organs, particularly those that rely on tissue remodeling.

Isidora Rovic and Jacqui Detmar contributed equally to this work.

Electronic supplementary material The online version of this article (https://doi.org/10.1007/s00441-019-03055-1) contains supplementary material, which is available to authorized users.

✉ Andrea Jurisicova
jurisicova@lunenfeld.ca

[1] Lunenfeld Tanenbaum Research Institute, Mount Sinai Hospital, Toronto, Ontario M5G 1X5, Canada

[2] Institute of Medical Sciences, University of Toronto, Toronto, Canada

[3] Present address: MedAvail Technologies Inc., 6810 Meadowvale Town Centre Circle, Unit 18, Mississauga, ON L5N 7T5, Canada

[4] Department of Physiology, University of Toronto, Toronto, Canada

[5] Department of Obstetrics and Gynecology, University of Toronto, Toronto, Canada

The placenta is a transient organ that undergoes extensive remodeling during its relatively short lifespan. This remodeling has been shown to be regulated, in part, by various mechanisms of PCD. For example, apoptosis in the placenta has been implicated in mediating trophoblast turnover. Specifically, the syncytiotrophoblast cells of the placental villi, which mediate fetal-maternal exchange, require constant replenishment of cellular content from the underlying "stem" cytotrophoblast cells. This process of renewal utilizes cellular machinery from the apoptotic cascade to promote cell-cell fusion of cytotrophoblast with syncytiotrophoblast. Activation of the cell death program is initiated in the villous cytotrophoblast cells, delayed during syncytialization and finalized just prior to the extrusion of apoptotic nuclei from syncytial cells, which are subsequently released as "debris" into the maternal circulation (Huppertz et al. 1998). Importantly, heightened trophoblast cell death has been associated with impaired syncytialization and exuberant syncytial debris shedding in placental disorders, such as PE and IUGR (Hung et al. 2012; Cali et al. 2013). In addition to regulating syncytialization, cell death has also been shown to be an important factor for the de novo formation of blood vessels (i.e., vasculogenesis) during human placentation (Tertemiz 2005).

Although an essential feature of placental development, the extent and pattern of cell death in the mouse placenta has been largely unexplored. Comparative studies of human and mouse placentae have demonstrated striking similarities in the molecular and cellular framework of this organ (Rossant and Cross 2001; Cox et al. 2009; Soncin et al. 2018). Between day 7.5 and 9.5 *post coitum* (d7.5–9.5), the developing ectoplacental cone (EPC) of the mouse conceptus undergoes major morphological remodeling, resulting in the formation of three distinct cellular regions that form the mature murine placenta (Rossant and Cross 2001). Fusion of the allantois with the chorion and subsequent branching, establishes a network of villi surrounded by small canals collectively referred to as the labyrinth. The labyrinth is the inner most region of the placenta, which is responsible for gas, waste and nutrient exchange between the mother and developing fetus. It is thus functionally analogous to the floating chorionic villi of the human placenta. The junctional zone (JZ) of the murine placenta consists of variable-sized spongiotrophoblast (SpT) cells with the capability of differentiating into secondary giant (TGCs) and glycogen (GlyTs) cells. Due to the expression of several gene markers, as well as their spatial distribution within the placenta, the cells of this region are considered to be analogous to human extravillous cytotrophoblast cells found in anchoring columns (Bouillot et al. 2006; Coan et al. 2006). Finally, trophoblast giant cells (TGCs) of the murine placenta invade the endometrium and are positioned in direct contact with the maternal decidua. Due to their invasive nature, murine TGCs are often compared to human interstitial extravillous trophoblast cells, which also invade into the interstitial space of the decidua. These cells have distinctively large, polyploid nuclei and are efficient in producing several key regulatory, luteotropic and lactogenic hormones, as well as angiogenic factors (Hu and Cross 2010). In addition, a subset of specialized murine TGCs are capable of remodeling maternal spiral arteries, a physiologically important event that also occurs during human placentation (Cross et al. 2002). It is important to note that murine TGCs do not invade as deeply into the maternal compartment as human interstitial extravillous trophoblast and thus the similarity between these two cell types has been contested. Perhaps a better murine counterpart would be GlyT cells, which, around mid-gestation in the mouse, migrate past the TGC barrier into the interstitial space of the decidua (Coan et al. 2006).

The mechanisms of cell death in the human placenta have been shown to be regulated by several B cell lymphoma 2 (Bcl-2) family members and caspase enzymes (Sharp et al. 2010). The Bcl-2 family of molecules includes both cell death inhibitors (Bcl-2, Bcl-X1, BCL-W, MCL-1 and A1) and cell death inducers. The latter is further divided into two subgroups—those which contain multiple Bcl-2 homology (BH) domains (Bax, Bak, Bok), or a single BH-3 domain (Hrk, Bim, Bad, Bik, Noxa and Puma). Bcl-2-related ovarian killer (Bok) is highly expressed in reproductive tissue and has been shown to be a key cell death regulator during normal human placentation (Soleymanlou et al. 2005; Ray et al. 2010; Kalkat et al. 2013; Melland-Smith et al. 2015). Furthermore, a splicing isoform of this protein and its full length isoform have both been implicated in the pathogenesis of preeclampsia (Soleymanlou et al. 2005; Soleymanlou et al. 2007; Ray et al. 2010). Bok overexpression in cultured trophoblast cells results in mitochondrial depolarization and increased caspase-3 cleavage, suggesting that Bok elicits apoptosis through the canonical caspase pathway in human trophoblast (Soleymanlou et al. 2005). In addition, Bok has been shown to be a potent inducer of autophagy in human embryonic kidney (HEK) cells by increasing lysosomal activity and autophagic flux (Kalkat et al. 2013). In light of the key roles played by Bok in human trophoblast, we sought to determine the expression levels and cellular distribution of this cell death molecule in the mouse placenta.

In the present study, we report the results of a systematic analysis of the temporal and spatial distribution of cell death in ICR and C57Bl/6 placentae throughout development. Both of these strains are frequently used as animal models for developmental and placentation studies. Given that variable phenotypes can manifest in genetically engineered mice on different genetic backgrounds (Linder 2006; Doetschman et al. 2009) and strain-specific differences were observed in toxicologically mediated cell death outcomes during murine pregnancy (Detmar et al. 2006; Detmar et al. 2008), a comparison between the two strains was deemed prudent. Our analysis revealed substantial differences in placental cell death rates

between these two strains. These findings may shed light on variable phenotypes observed in genetic mutants developed on different strains.

Materials and methods

Animal housing, mating and tissue collection

Six-week-old ICR (Harlan, Indianapolis, IN, USA) and C57Bl/6 (National Cancer Institute, Frederick, MD, USA) virgin females were mated with the appropriate male stud (i.e., ICR or C57Bl/6) of proven fertility. Gestational age was determined based on the presence of a vaginal plug, with the morning of detection designated as day 0.5. Animals were maintained in a controlled room with a 12-h light: 12-h dark cycle and allowed ad libitum access to rodent chow and water.

At gestational days 7.5–18.5, placentas from ICR and C57Bl/6 females were collected and either frozen for protein assays or fixed in 10% phosphate-buffered formalin for histological analysis. Decidual tissue was removed from d7.5 and d8.5 EPC and discarded, while the decidua was left intact on d9.5–d18.5 placentae. Ectoplacental cones from the same dam were pooled in order to have enough tissue for immunoblotting analyses. All animal experiments were conducted using protocols approved by the TCP Animal Care Committee.

Terminal deoxynucleotidyl transferase dUTP nick-end labeling

Three healthy conceptuses (d7.5) or placentae (d9.5–d11.5, d13.5, d15.5 and d18.5) from three different ICR or C57Bl/6 dams were embedded in paraffin using routine histological techniques. Conceptuses from d7.5 were embedded whole, while later-gestation placentae were cut slightly lateral to the midline and the larger half was embedded to obtain transverse sections. All tissue blocks were serially sectioned at 5 μm thick and sections corresponding to the midline, 50 μm and 100 μm, were chosen for TUNEL staining as previously described (Detmar et al. 2008) with a few source modifications: Proteinase K (cat# PRK403; Bioshop, Burlington, Canada), TdT (cat# 11279121; Roche, Indianapolis, USA), NEBuffer 4 (cat# B7004S; BioLabs, MA, USA) and dUTP (cat# 14687530; Roche, Indianapolis, USA) for TdT reaction. For positive control, tissue was digested with DNase I (cat# D5307; Sigma, MO, USA) for 10 min at RT and for negative control, TdT enzyme was excluded from the reaction (Fig. S1). Histomorphometric analyses were performed only on placental sections that exhibited appropriate morphology, with all three placental layers discernible. A Zeiss 9901 microscope, a Retiga 1300 camera and a BioQuant® Software microscope were used for analysis, with the researcher blind to the strain of mouse and gestational time point. TUNEL-positive cells were counted at × 500 magnification, scanning the entire section. For d7.5 tissue, TUNEL-positive cells were counted in three regions: mesometrial decidua, anti-mesometrial decidua and ectoplacental cone (EPC). All TUNEL-positive TGCs and allantoic cells were counted in the entire conceptus. For all other gestational time points, TUNEL-positive cells were counted in four separate regions: the chorionic plate (CP), labyrinthine, junctional zone (area between the labyrinth and giant cell border) and the maternal compartment (area between the giant cell border and the myometrium). All TUNEL-positive TGCs were counted in the entire placenta, except for those contained within the extreme lateral edges of the placenta, adjacent to the decidua parietalis. If a group of dead cells in the maternal compartment contained greater than nine TUNEL-positive cells, these were considered to be focal points of death and the area of these foci was determined at × 500 magnification. The rate of this type of death was expressed as a percent of the area exhibiting TUNEL staining over the total area of the tissue in the maternal compartment. Photomicrographs were taken using a Leitz DMRXE microscope, a Sony DXC-970MD camera and Northern Eclipse® software.

Immunohistochemistry

Sections were treated for immunohistochemistry as previously described (Detmar et al. 2008). Anti-active-caspase-3 antibody (1:500; Cell Signaling, cat# 9662) and Bok_{2099} IgG generated in-house (5 μg/ml; Soleymanlou et al. 2005; Ray et al. 2010) were diluted in 5% horse serum + 5% BSA in PBS. In addition, antibody depletion of Bok using the peptide antigen was performed to assess antibody specificity. Briefly, 25 μg of IgG was incubated with excess peptide overnight at 4 °C, with gentle shaking; a control tube containing IgG, to which no peptide had been added, was also included. The samples were then centrifuged at 20,000*g* for 30 min at 4 °C and the supernatant was collected and used for IHC or Western blotting.

Caspase-3 enzyme assay

Enzymatic activity of caspase-3 in murine placental tissues was assessed using the Caspase-3 Cellular Activity Assay Kit PLUS (Biomol, Plymouth Meeting, PA, USA). Briefly, d15.5 placentae from both ICR and C57Bl/6 mice (1 placenta each from $n = 4$ dams) were dissected into either maternal-enriched (decidua) or fetal-enriched (labyrinth and spongiotrophoblast) fractions, weighed and homogenized in cell lysis buffer at a ratio of 1 mg tissue: 5 μl lysis buffer. A total of 25 μg of protein lysate was used for each sample in the assay. Thereafter, the assay was performed according to the manufacturer's protocol, using the colorimetric, pNA substrate provided. Absorbance readings were done at 10-min intervals for a total of 120 min. Calculation of enzymatic

activity was done using the slope of the linear portion of the time course.

Western blotting

To assess protein expression in ICR and C57Bl/6 placentae, two to three placentae from three separate dams were pooled and lysed in 1× SDS sample buffer and treated for Western blotting as previously described (Detmar et al. 2008). The following primary antibodies were used: anti-caspase-3 (1:500; Cell Signaling, cat# 9662), Bok IgG (5 μg/ml) and anti-cleaved Parp-1 (1:500, Cell Signaling, cat# 9544). Blots were stripped and reprobed with anti-β-actin antibody (1:400, Santa Cruz, cat# sc-1616) to correct for protein loading. The appropriate alkaline phosphatase-conjugated secondary antibody (1:1000 anti-rabbit antibody; BioRad, cat# 170-6518 or 1:1000 anti-goat antibody; Santa Cruz, cat# sc-2771) was used for detection of the primary antibody. After washing, membranes were incubated with ECF substrate (GE Healthcare) and scanned on a STORM imager (Molecular Devices). Densitometric analyses were done using ImageQuant® software.

Statistical analysis

ICR and C57Bl/6 pup weights, placental weights and litter sizes were analyzed by an unpaired *t* test and a Mann-Whitney test for parametric and non-parametric data, respectively. Parp-1 cleavage profiles over gestation within one strain and between the two strains were analyzed by one-way and two-way ANOVAs, respectively. Post hoc comparisons of means were analyzed using the Bonferroni test. The statistical software used was GraphPad PRISM (Version 5.0a) and data were considered statistically significant if $P \leq 0.05$. For all other analyses, ICR and C57Bl/6 placental cell death rates and protein expression levels were analyzed by one-way and two-way ANOVAs over gestation within one strain and between the two strains, respectively. Post hoc comparisons of means were analyzed using the Tukey-Kramer test. The statistical software used was SPSS® (Version 13) and data were considered statistically significant if $P \leq 0.05$. All results are expressed as the mean ± standard error (SE).

Results

Reduced fetal growth and litter sizes of C57Bl/6 mice

A putative IUGR phenotype of C57Bl/6 fetuses has been previously proposed (Rennie et al. 2012). In the present study, we confirmed that C57Bl/6 fetuses exhibit a significant reduction in total body weight at d17.5 (~ 20%), compared to ICR fetuses (Fig. 1a). No difference in average placental weight (Fig. 1b) or number of resorptions per liter at d17.5 was observed (data not shown). C57Bl/6 neonates had a 25% reduction in body weight (Fig. 1c) and litters from this strain were significantly smaller compared to ICR litters (Fig. 1d). No sex differences in neonatal weights were observed for either strain (Fig. 1e). Taken together, these results demonstrate that fetuses from the inbred C57Bl/6 strain display developmental growth delays indicative of an IUGR phenotype, as previously reported.

ICR and C57Bl/6 conceptuses and decidua display similar numbers and patterns of TUNEL positivity at d7.5

At gestational day 7.5 (d7.5), regions demonstrating the greatest number of TUNEL-positive cells were the mesometrial and anti-mesometrial decidual cells—adjacent to the EPC and distal endoderm, respectively. Similar rates of TUNEL-positive cells were observed in all three regions in ICR and C57Bl/6 placentae (Fig. 2a). Interestingly, the anti-mesometrial decidua of both strains exhibited significantly higher rates of cell death compared with that seen in the mesometrial decidua (Fig. 2a). Additionally, the uterine cavity often contained TUNEL-positive detached cells and debris (Fig. 2b). The EPC exhibited sporadic cell death, with no discernible pattern (Fig. 2c, left panel), while TUNEL-positive primary TGCs were concentrated on the anti-mesometrial pole (Fig. 2c, right panel). Most of these primary TGCs displayed condensing nuclei and exhibited morphological signs of death, yet were TUNEL-negative (Fig. 3a). Moreover, both strains showed a greater percentage of TUNEL-negative, chromatin-condensing primary TGCs, compared with the characteristic TUNEL-positive cells typically observed at mid- to late-gestation (Fig. 3a). Lastly, several primary TGCs contained TUNEL-positive cell remnants (corpses), which were likely engulfed by these cells during phagocytosis (Fig. 3b). Overall, the patterns of TUNEL positivity for the various cell types in the regions studied (i.e., mesometrial and anti-mesometrial decidua, EPC and primary TGCs) at d7.5 were comparable for both ICR and C57Bl/6 mouse strains.

ICR and C57Bl/6 placentas exhibit differences in the patterns and frequency of cell death from d10.5–d18.5

Trophoblast giant cell: d10.5–d18.5

Different morphological features of trophoblast giant cell (TGC) death were observed across gestation, including (1) TGCs with condensing, TUNEL-positive nuclei; (2) TGCs with TUNEL-negative nuclei but condensing chromatin and cell shrinkage; and (3) healthy TGCs containing phagocytosed, TUNEL-positive corpses.

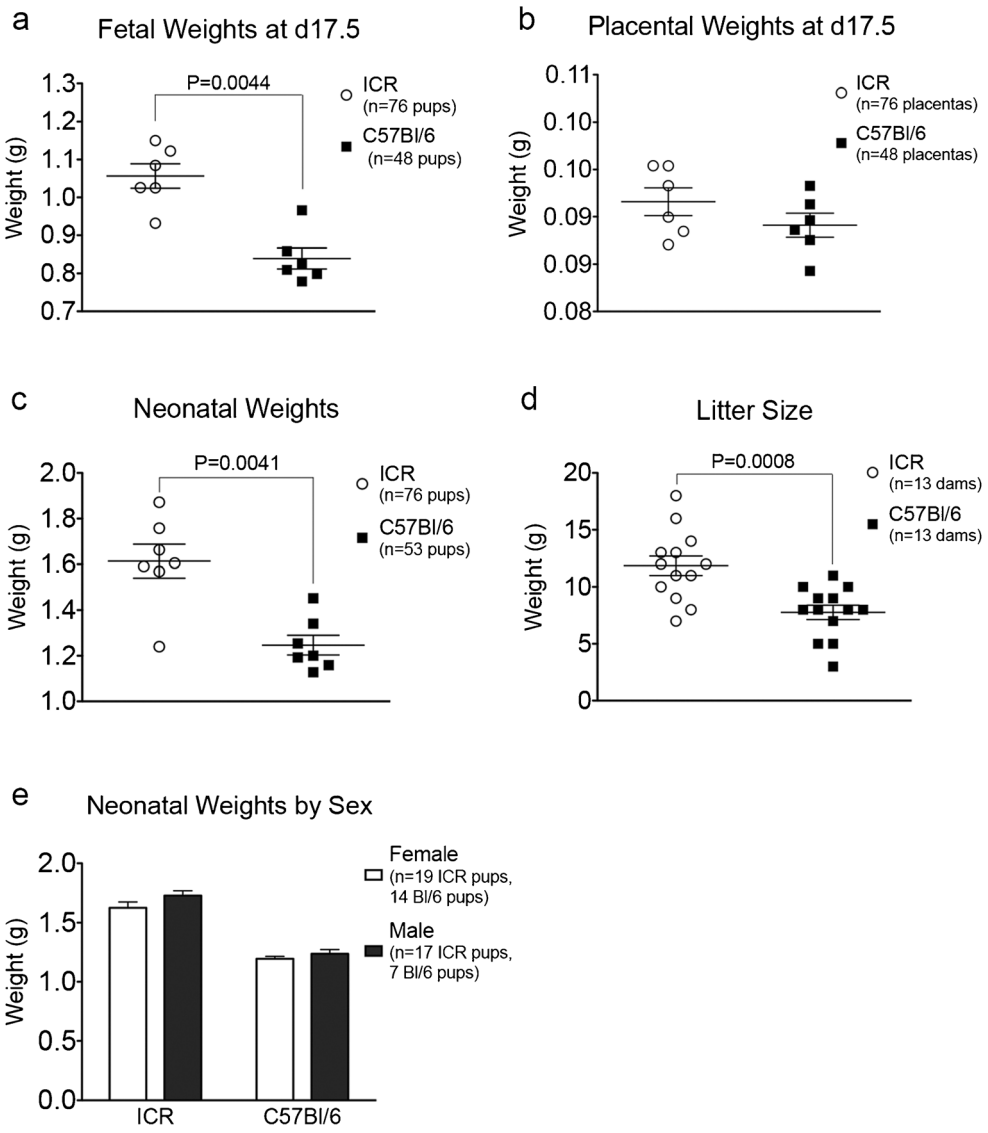

Fig. 1 Developmental differences in ICR and C57Bl/6 mice. Fetal weights (**a**), placental weights (**b**), neonatal weights (**c**), litter sizes (**d**) and neonatal weights by sex (**e**) for each strain are shown as average values ± SE. Each point represents a dam and the total number of pups are indicated in the corresponding figure legends. Statistical significance was measured using a *t* test or Mann-Whitney test for parametric and non-parametric data, respectively, with *n* being the number of dams. Values of significant statistical difference are shown with corresponding *P* value

At d10.5, the percent of cell death within all three groups of TGCs appeared approximately equal (Fig. 3a, b). However, this pattern changed beginning at d13.5, with the majority of TGCs exhibiting condensing, TUNEL-positive nuclei (type 1) (Fig. 3a). Near the end of gestation (d15.5–d18.5), there was a trend towards increased rates of type 1 TGCs in both strains; however, it was more prominent in C57Bl/6 placentae (Fig. 3a). Neither strain exhibited profound differences in the rate of condensing, TUNEL-negative TGC death (type 2). Finally, the percent of TGCs containing TUNEL-positive cell corpses (type 3) remained relatively consistent over time, with a small but significant decrease in both strains observed over gestation (Fig. 3b).

Chorionic plate: d10.5–d18.5

TUNEL-positive cells were observed in the chorionic plate (CP) at all gestational time points and increased as gestation progressed (Fig. 4a). The majority of cell death occurred sporadically throughout the CP, with some clustering of TUNEL-positive cells around the smaller blood vessels. Importantly, the CP of C57Bl/6 placentae contained greater numbers of TUNEL-positive cells compared with the CP of ICR placentae; however, this was statistically significant only at mid-gestation (d13.5 and d15.5) (Fig. 4a).

Labyrinth: d10.5–d18.5

At d10.5, no difference in the number of TUNEL-positive cells between the ICR and C57Bl/6 labyrinth region was observed (Fig. 4b). However, from d13.5 to d18.5, the C57Bl/6 labyrinth exhibited a significantly increased number of TUNEL-positive cells compared to ICR (Fig. 4b). The majority of dead/dying cells were lining the fetal capillaries and maternal blood spaces. As gestation progressed, there was a general shift from sporadic cell death (Fig. 4b, upper panel) to

clustered death (Fig. 4b, lower panel) observed in the labyrinth of both strains of mice.

SpT tissue appeared insinuated within the labyrinth region, often completely mixing with GlyT by d18.5. From d15.5 to d18.5, there was a significantly greater number of dead cells in the C57Bl/6 SpT region, compared with ICR (Fig. 4c). The majority of TUNEL-positive SpT/GlyT cells within the labyrinth region were directly adjacent to large, maternal blood canals (Fig. 4c).

Junctional zone: d10.5–d18.5

The cells of the JZ in both strains exhibited increasing rates of TUNEL positivity from d13.5 to term (Fig. 5a). Interestingly, the JZ of ICR placentae contained higher numbers of TUNEL-positive cells from d13.5–d17.5. In addition, GlyT cells of the JZ in ICR placentae demonstrated focal regions or "pockets" of cell death at the maternal-fetal interface beginning at d15.5 (Fig. 5a), while C57Bl/6 placentae did not demonstrate these patterns until d17.5.

The maternal compartment: d10.5–d18.5

At mid-gestation, TUNEL-positive cells were scattered within the maternal compartment. The number of sporadic TUNEL-positive cells in the maternal compartment increased across gestation for both mouse strains studied; however, there were significantly more of these scattered dead and/or dying cells in C57BL/6 placentae (Fig. 5b).

At d15.5, focal regions of TUNEL positivity were observed surrounding the maternal vessels at the maternal-fetal (M-F) interface in placentas of both strains (Fig. 5c). For ICR placentae, the peak percent of clustered cell death in this region occurred at d17.5, followed by a dramatic decrease at d18.5 (Fig. 5c). In C57Bl/6 placentae, a similar clustering of dead/dying cells around the maternal blood vessels occurred; however, the percentage of TUNEL-positive foci in the maternal compartment of C57Bl/6 placentae was significantly lower than those in ICR placentae at all time points examined (Fig. 5c).

Caspase-3 expression and localization are similar for ICR and C57Bl/6 placentae

Activation of caspase-3 is considered to be a hallmark feature of cell death by apoptosis. Thus, we determined the levels of cleaved caspase-3 in ICR and C57Bl/6 placentas across gestation by western blotting. Both ICR and C57Bl/6 placental lysates exhibited similar levels of cleaved caspase-3 protein expression, which peaked at early- to mid-gestation (d9.5–d11.5) and gradually decreased over the remaining developmental time points (d13.5–d18.5) (Fig. 6a). In addition, caspase-3 enzyme assays revealed significantly higher caspase activity in fetal-enriched (labyrinth and spongiotrophoblast), compared with maternal-enriched (decidual) fractions of d15.5 placentae, for both strains examined (Fig. 6b). While both fetal-enriched and maternal-enriched placental lysates of C56Bl/6 origin displayed higher levels of caspase-3 activity than ICR placentae, this difference did not reach statistical significance. Immunohistochemical analysis using cleaved-caspase-3 antibody on d15.5 placental sections resulted in patterns of reactivity that were comparable to those seen using TUNEL, namely positive cells concentrated around fetal vessels in the labyrinth and around maternal vessels at the maternal fetal interface (Fig. 6d).

Fig. 2 Cell death patterns in d7.5 ICR and C57Bl/6 conceptuses. **a** Number of TUNEL-positive cells per 100 μm^2 of tissue. **b** Photomicrograph demonstrating the uterine cavity of a d7.5 ICR conceptus, containing TUNEL-positive debris and nuclei (indicated by black arrow). Mesometrial and anti-mesometrial poles of conceptus are indicated. Low- (**c**) and high-magnification (**c'**) photomicrographs of d7.5 ICR EPC, with arrow indicating TUNEL-positive trophoblast cell within EPC. Low- (**d**) and high-magnification (**d'**) photomicrographs of d7.5 embryo, surrounding primary TGCs and anti-mesometrial decidua. Filled arrowheads indicate TUNEL-positive primary TGCs and unfilled arrowheads indicate healthy primary TGC nuclei. Bars represent average values ± SE, with white and black bars denoting TUNEL positivity in ICR placentae ($n = 8$) and C57Bl/6 placentae ($n = 6$), respectively. Values of significant statistical difference between different tissue regions are shown with corresponding P value (Tukey-Kramer post hoc test)

Parp-1 cleavage patterns are different for ICR and C57Bl/6 placentae

Cleavage of poly (ADP-ribose) polymerase 1 (PARP-1) by caspases is another common feature of apoptosis. We therefore examined the protein expression pattern of Parp-1 throughout gestation for both strains. The cleavage profile of Parp-1 consistently demonstrated a lack of the classical 89 kDa fragment and instead exhibited Parp-1 proteolytic products of approximately 75 and 52 kDa. Levels of 75 kDa Parp-1 gradually declined in ICR placentae over gestation, while in C57Bl/6 placentae, this cleavage product peaked at d11.5, exhibiting significantly higher levels compared to ICR (Fig. 6c). On the other hand, levels of 52 kDa Parp-1 demonstrated much more variable expression between the two strains. In C57Bl/6 placentae, 52 kDa Parp-1 peaked at d15.5, exhibiting significantly higher levels compared to ICR (Fig. 6c). In ICR placenta, this cleavage product increased after d9.5 and was significantly higher than C57Bl/6 at both d11.5 and d18.5.

Bok is expressed in murine trophoblast and at different levels in ICR and C57Bl/6 placentae

The pro-apoptotic Bcl-2 protein Bok has been implicated in the regulation of trophoblast proliferation and death in the

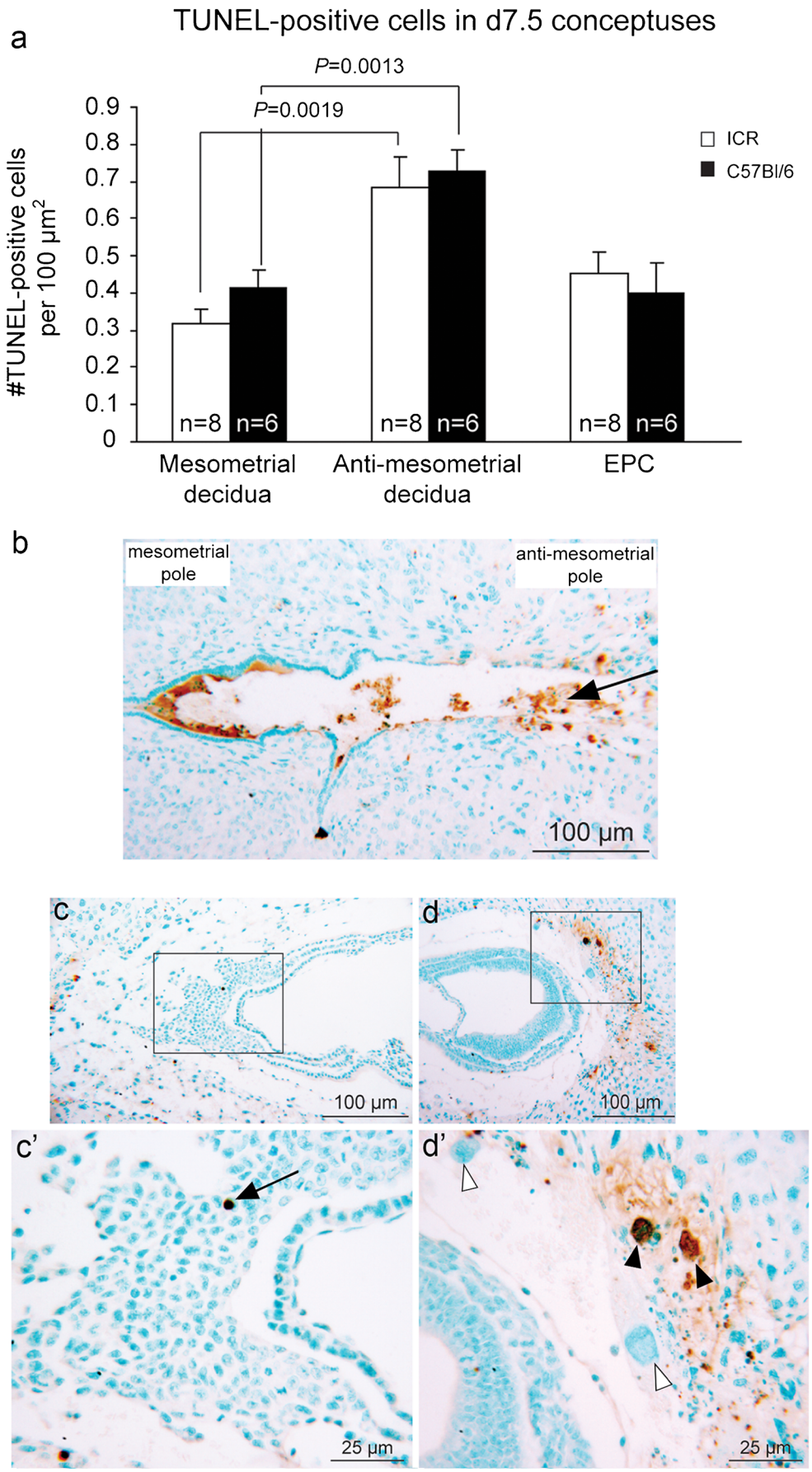
a
TUNEL-positive cells in d7.5 conceptuses
P=0.0013
P=0.0019
#TUNEL-positive cells per 100 µm2
0.9
0.8
0.7
0.6
0.5
0.4
0.3
0.2
0.1
0
ICR
C57Bl/6
n=8
n=6
n=8
n=6
n=8
n=6
Mesometrial decidua
Anti-mesometrial decidua
EPC
b
mesometrial pole
anti-mesometrial pole
100 µm
c
100 µm
d
100 µm
c'
25 µm
d'
25 µm

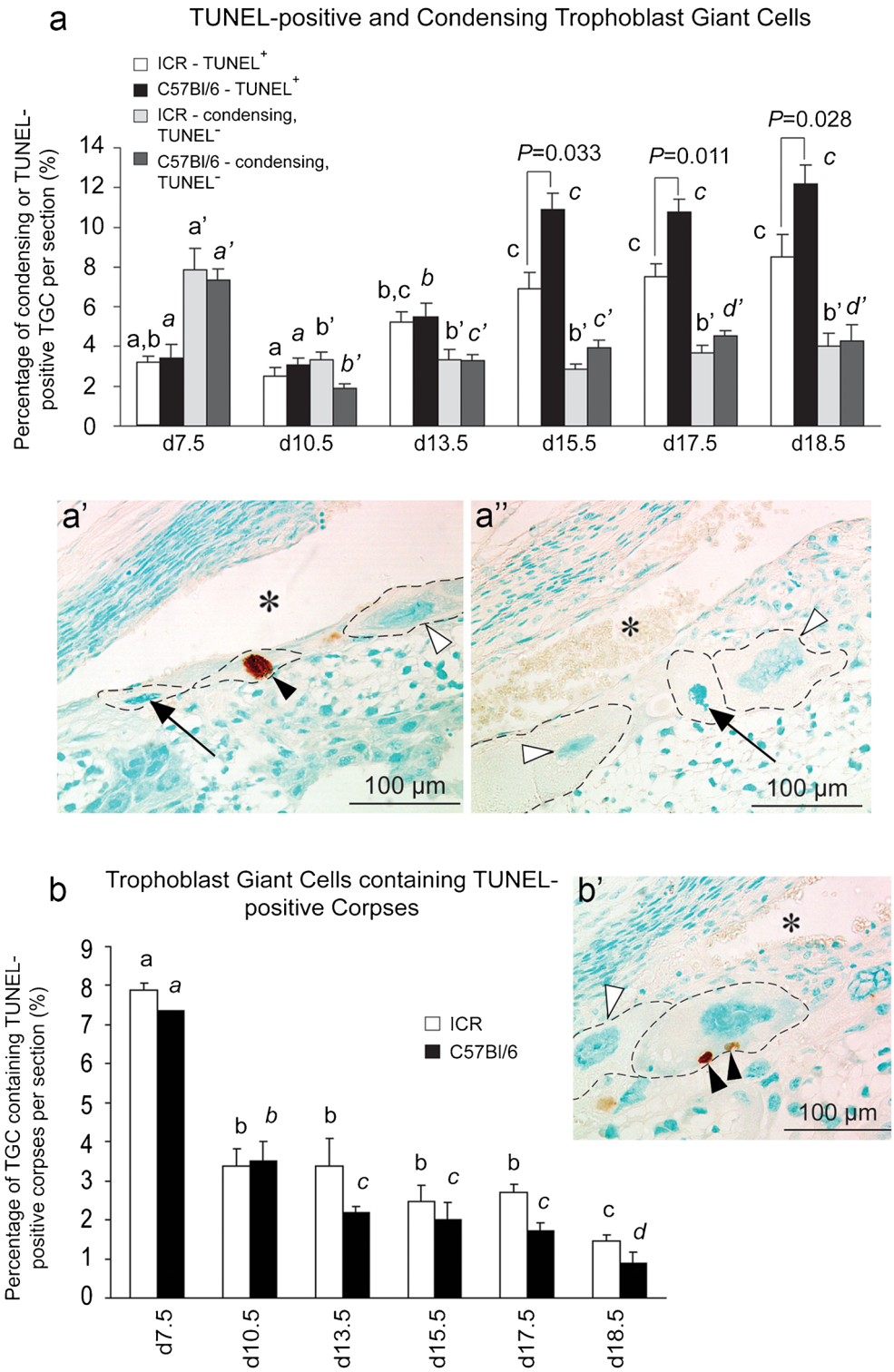

Fig. 3 Trophoblast giant cell death patterns in ICR and C57BL/6 placentae over gestation. **a** Percentage of TUNEL-positive ($TUNEL^+$) and condensing TGCs ($TUNEL^-$) per placental section in ICR and C57Bl/6 placentae over gestation. **a'**, **a"** TUNEL-positive (arrowhead) and condensing (arrows) TGC nuclei in d15.5 ICR placentae (cell borders indicated by dashed line); open arrowheads indicate healthy TGC nuclei and asterisks (*) indicate maternal vessels. **b** Percentage of TGC containing TUNEL-positive corpses in ICR and C57Bl/6 placentae over gestation. **b'** TGC containing two TUNEL-positive corpses (arrowheads) within the cytoplasm. Healthy TGC, without cell corpses is indicated by the open arrowhead. Bars represent average values ± SE, with white and black bars denoting TUNEL positivity in ICR placentae ($n_{d7.5} = 8$, $n_{d10.5} = 8$; for all other time points, $n = 9$) and C57Bl/6 placentae ($n_{d7.5} = 6$, $n_{d10.5} = 8$; for all other time points, $n = 9$), respectively. Within the same strain over gestation, means with the same letter are not significantly different from each other (Tukey-Kramer test, $P < 0.05$). Values of significant statistical difference between ICR and C57Bl/6 placentae are shown with corresponding P value (Tukey-Kramer test)

human placenta (Soleymanlou et al. 2005; Ray et al. 2010). We therefore examined its expression in the mouse placenta across gestation. Western blotting against total placental lysates, using a polyclonal antibody produced in house (Bok_{2099}), yielded a predominant band at approximately 28/30 kDa, consistent with the reported 28 kDa molecular weight of human placental Bok (Soleymanlou et al. 2005). Additionally, high molecular weight bands at 45–55 kDa were observed and all immunoreactive bands disappeared after treatment with peptide antigen-depleted antibody (Fig. 7a). Further assessment of antibody specificity after Western blotting of tagged, recombinant, rat Bok protein (R&D Systems)

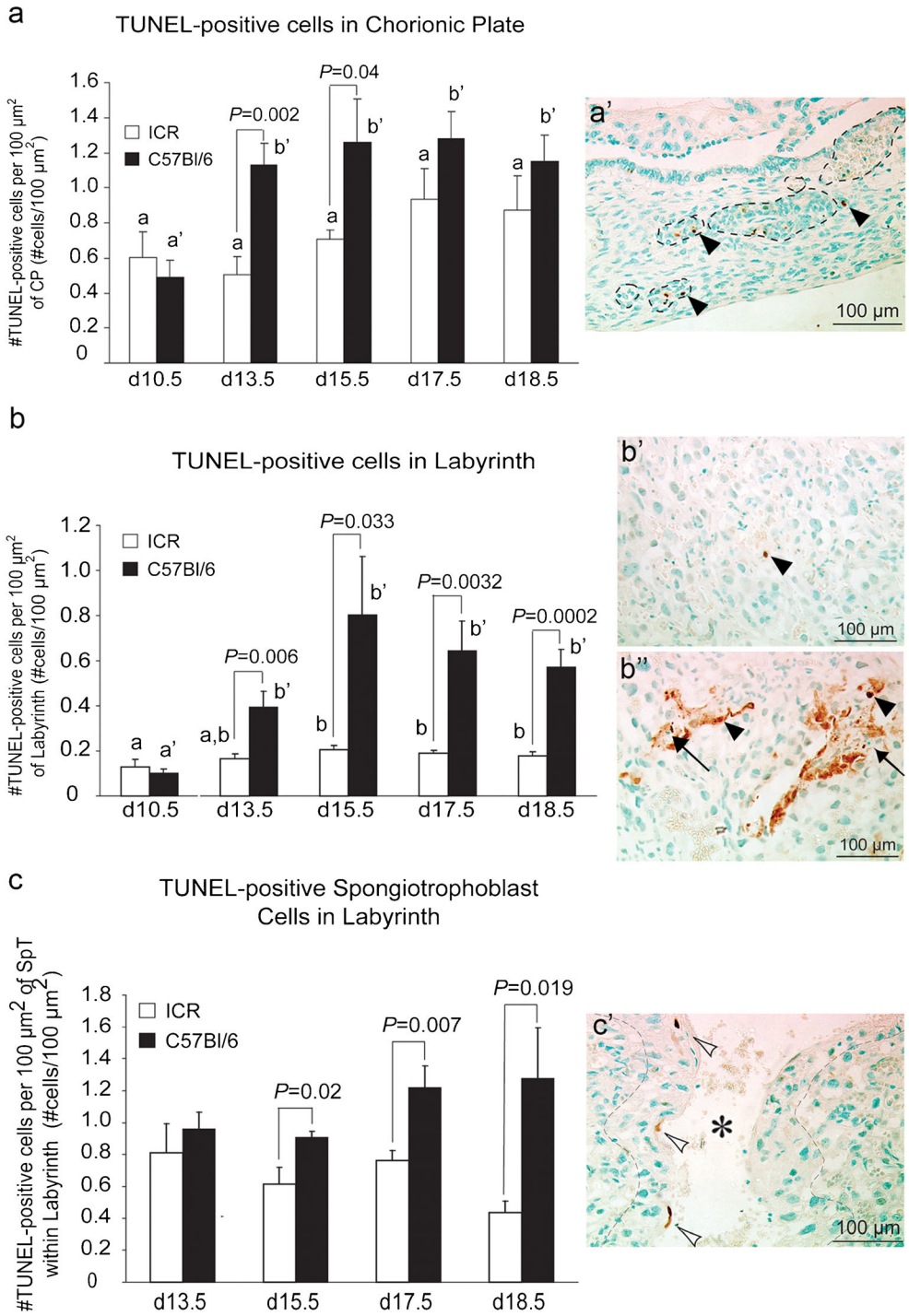

Fig. 4 TUNEL patterns in ICR and C57Bl/6 chorionic plate and labyrinth over gestation. **a** Number of TUNEL-positive nuclei per 100 µm^2 of CP over gestation. **a'** Representative picture of typical TUNEL-positive nuclei in d15.5 CP; arrowheads indicate TUNEL-positive CP nuclei and dotted lines outline vessels. **b** Number of TUNEL-positive nuclei per 100 µm^2 of labyrinth over gestation. **b'** Sporadic TUNEL positivity seen in d15.5 labyrinth. **b"** Typical cell death patterns seen along the labyrinthine vessels. Arrowheads indicate TUNEL-positive labyrinth nuclei and arrows indicate nucleated fetal red blood cells within dying/dead vessel. **c** Number of TUNEL-positive nuclei per 100 µm^2 of spongiotrophoblast within the labyrinth layer. **c'** Accompanying photomicrograph depicts characteristic TUNEL patterns observed in trophoblast cells of this tissue. Dotted lines indicate the border between the labyrinth and the spongiotrophoblast surrounding the maternal blood canal, indicated by asterisk (*); empty arrowheads indicate TUNEL-positive nuclei in trophoblast cells encircling the maternal blood. For all graphs, white bars represent average values for ICR placentae ($n = 9$ for all time points except $n_{d10.5} = 8$) and black bars represent average values for C57Bl/6 placentae ($n = 9$ for all time points except $n_{d10.5} = 8$) ± SE. Within the same strain over gestation, means with the same letter are not significantly different from each other (Tukey-Kramer test, $P < 0.05$). Values of significant statistical difference between ICR and C57Bl/6 placentae are shown with corresponding P value (Tukey-Kramer test)

confirmed reactivity of our antibody (data not shown). As depicted in Fig. 7(b), both ICR and C57Bl/6 placentae displayed comparable levels of Bok at d10.5. However, from d13.5 to d17.5, C57Bl/6 placentae maintained a consistent significantly lower level of Bok expression (28 kDa form) compared to ICR placentae.

Bok immunolocalization was examined throughout placental development, with antibody specificity being confirmed by peptide-antigen-depletion (Fig. 7a). Expression of Bok was observed in parietal TGCs and spongiotrophoblast cells of the junctional zone in both strains (Fig. 7c, left panel). Healthy TGCs exhibited light cytoplasmic/perinuclear staining, while early-dying TGCs exhibited more intense staining with positive nuclei (Fig. 7c, right panel). In addition, both nuclear and cytoplasmic Bok staining was also observed in pockets of GlyT (Fig. 7c). Lastly, within the labyrinth, a subset of sinusoidal TGCs and syncytiotrophoblast cells exhibited perinuclear Bok staining (Fig. 7d). A summary of cell death patterns throughout development of the mouse placenta is presented in Fig. 8.

Fig. 5 Fetal spongiotrophoblast and maternal compartment cell death patterns in ICR and C57BL/6 placentae at specified time points over gestation. **a** Number of TUNEL-positive nuclei per 100 μm^2 of junctional zone tissue over gestation. **a'** Representative picture of typical TUNEL-positive nuclei in d15.5 junctional zone. Dotted line delineates the border between the labyrinth and the spongiotrophoblast layer of the junctional zone; arrowheads indicate TUNEL-positive spongiotrophoblast nuclei. **b** Number of sporadic, TUNEL-positive nuclei within the maternal compartment of ICR and C57Bl/6 placentae over gestation. **b'** Region of maternal decidua with sporadic, TUNEL-positive nuclei (arrowheads). **c** Percentage of area in the maternal compartment that exhibits focal regions of TUNEL positivity for ICR and C57Bl/6 placentae over gestation. **c'** Maternal vessel (demarcated by dotted line) in maternal compartment, surrounded by foci of TUNEL-positive nuclei and acellular tissue. Solid line represents one of the focal areas of TUNEL positivity. Asterisk (*) represents a patch of acellular material. Bars represent average values ± SE, with white and black bars denoting TUNEL positivity in ICR placentae ($n_{d7.5} = 8$, $n_{d10.5} = 8$; for all other time points, $n = 9$) and C57Bl/6 placentae ($n_{d7.5} = 6$, $n_{d10.5} = 8$; for all other time points, $n = 9$), respectively. Within the same strain over gestation, means with the same letter are not significantly different from each other (Tukey-Kramer test, $P < 0.05$). Values of significant statistical difference between ICR and C57Bl/6 placentae are shown with corresponding P value (Tukey-Kramer test)

Discussion

Although cell death in the developing human placenta has been the subject of intense investigation, very little is known about the extent and patterns of cell death in the mouse placenta during pregnancy. The existence of homologous cell types and cellular behavior between these two species highlights the use of the mouse as a suitable model for the study of human placentation (Georgiades et al. 2002). In addition, the use of murine models allows for better temporal monitoring of molecular events occurring throughout placental development; as early as the d7.5 conceptus. Given that the mouse is the most commonly used animal model for placental research, an analysis of cell death patterns and underlying molecular pathways governing placental cell death in this species is crucial. Our current study determined that cell death in the mouse placenta exhibits similar patterns to what has previously been observed in the human placenta (Smith et al. 1997; Smith et al. 2000). That is, cell death appears comparatively infrequently during early placental development, giving way to a greater number of and more organized patterns of dying cells towards the end of gestation. In addition, different patterns of cell death (i.e., sporadic and clustered) were observed in various placental regions and cell types throughout gestation. Finally, we observed differences in the pattern and frequency of placental cell death between ICR and C57Bl/6 mouse strains. The results from this study can aid in the study and interpretation of various genetic models and pathological conditions of both the human and rodent placenta.

Programmed cell death (PCD) has been shown to play an important role in embryonic development, shaping organs such as the heart, digits and brain (Penaloza et al. 2006; Fuchs and Steller 2011). It has also been implicated in regulating human placental morphogenesis (Huppertz and Kingdom 2004). Throughout life, PCD also functions to promote neovascularization in nascent or newly functioning tissues, or to allow for vessel regression and occlusion after birth in the postpartum uterus (Dimmeler and Zeiher 2000). In fact, heightened expression of cell death mediators (i.e., cleaved caspase-3) has been observed in the postpartum mouse uterus, indicating that cell death is an important mechanism that facilitates parturition (Kyathanahalli et al. 2013). In the current study, TUNEL labelling of placenta sections revealed "pockets" of TUNEL-positive cells that emerged at d15.5, adjacent to the maternal-fetal interface in both strains of mice. A number of these TUNEL-positive foci clustered around the large maternal blood canals, suggesting that this organized pattern of cell death would facilitate clean separation of the placenta from the uterine wall upon parturition, thereby protecting the mother and fetus from excessive blood loss during delivery. Importantly, the trend towards decreased focal regions or "pockets" of cell death observed in inbred C57Bl/6 placentae could be suggestive of a developmental delay in placental maturation. Since fetuses of C57Bl/6 mice are known to exhibit growth curves indicative of compromised fetal growth, similar to IUGR (Kulandavelu et al. 2006; Rennie et al. 2012), it is possible that the regions adjacent to the maternal-fetal interface in this strain have not yet received the appropriate cell death cues for efficient parturition.

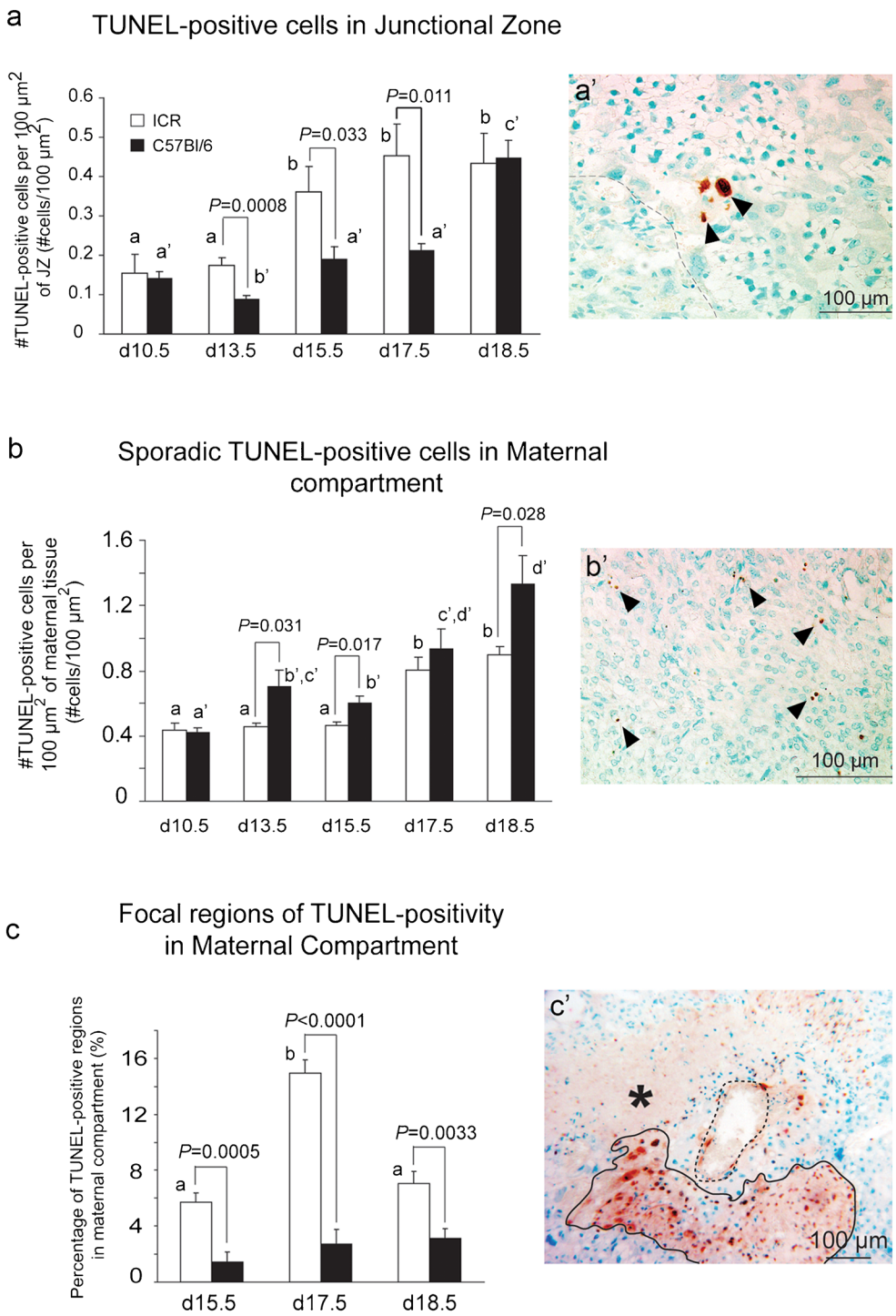

Cell death has been observed in the human placental labyrinth and is believed to be a driving factor for vasculogenesis (Tertemiz 2005). In the mouse placenta, we observed increased cell death throughout gestation in the labyrinth region of both ICR and C57Bl/6 strains. This observed death peaked at d15.5, with TUNEL-positive cells concentrating along the labyrinthine blood vessels (fetal and maternal). For both strains, cell death in the labyrinth was slightly reduced by d18.5. This "peak and decline" of cell death in the labyrinth could be a reflection of the massive vascular remodeling that takes place at mid-gestation, which serves to meet increasing fetal demand towards term (d18.5) (Rennie et al. 2012). Importantly, C57Bl/6 placentae displayed significantly greater numbers of TUNEL-positive cells in the labyrinth region at d15.5, compared to ICR placentae. A possible explanation for this may be a placental

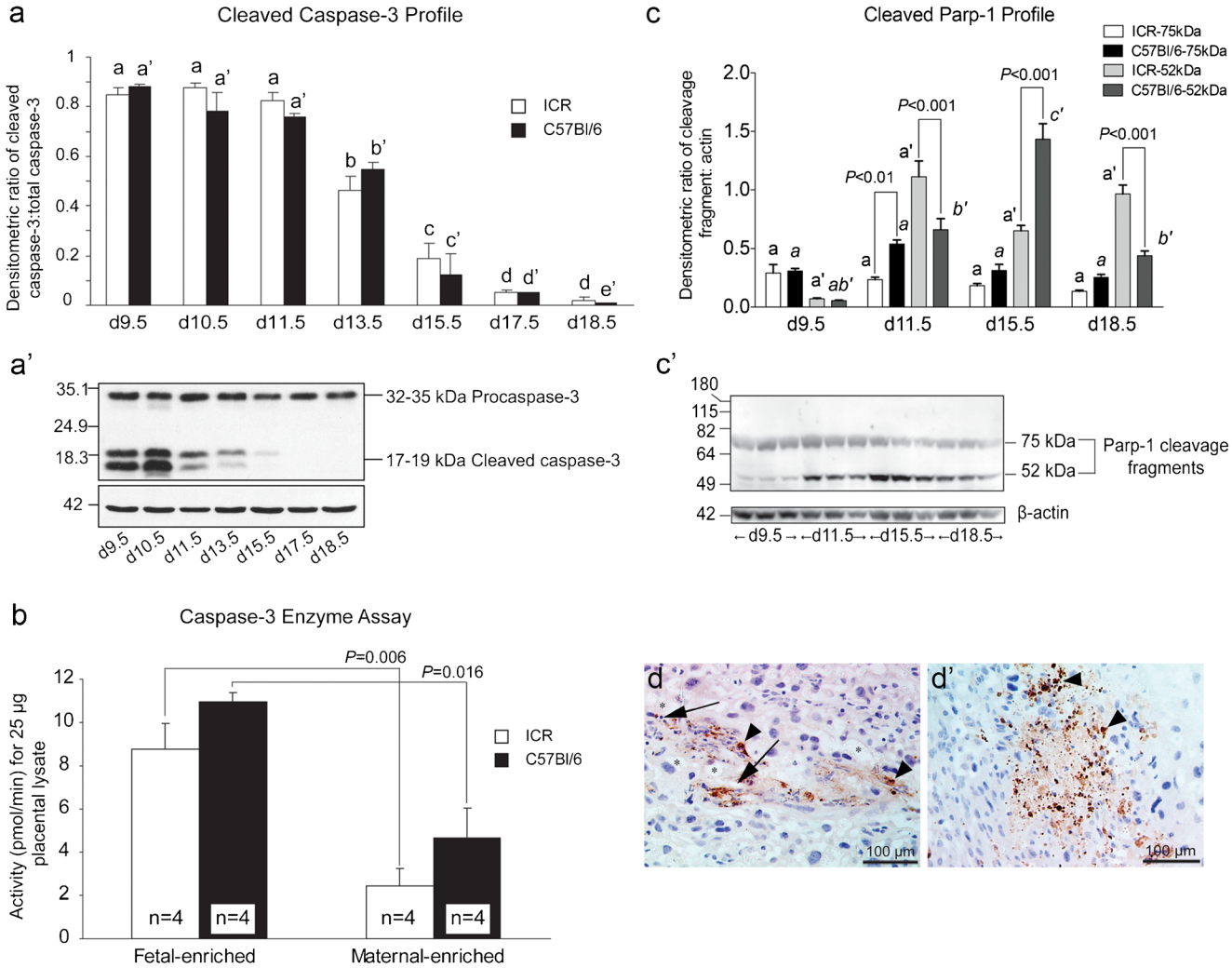

Fig. 6 Caspase-3 expression and activity in ICR and C57Bl/6 placentae are similar over gestation. **a** Procaspase-3 cleavage in placental lysates as a densitometric ratio of cleaved caspase-3: total caspase-3 over gestation, after Western blotting. **a'** Representative immunoblot of placental lysates from the indicated time points, against anti-caspase-3 and anti-β-actin antibodies. **b** Differences in caspase-3 activity between fetal and maternal compartments for ICR and C57Bl/6 placentae at d15.5. **c** Production of cleaved Parp-1 fragments at 75 kDa and 52 kDa over gestation. **c'** Representative immunoblot of placental lysates against anti-cleaved-Parp-1 and anti-β-actin antibodies. Parp-1 cleavage fragments at 75 and 52 kDa are indicated and arrow represents the putative position of the 89 kDa fragment. Representative photomicrographs of fetal labyrinth (**d**) and maternal compartmental placental tissue (**d'**) in d15.5 C57Bl/6 placenta, after cleaved caspase-3 immunohistochemistry. Arrowheads indicate cells positive for cleaved caspase-3, arrows indicate nucleated fetal red blood cells within positively stained labyrinthine vessels and asterisks (*) demarcate maternal blood spaces. Bars represent average values ± SE and $n = 3$ for both ICR and C57Bl/6 placentae. Within the same strain over gestation, means with the same letter are not significantly different from each other (Tukey-Kramer test, $P < 0.05$). Values of significant statistical difference between ICR and C57Bl/6 placentae are shown with corresponding P value (Tukey-Kramer test)

response to reduced fetal growth by upregulating vascular remodeling, leading to increased cell death. On the other hand, enhanced labyrinthine death in C57Bl/6 mice may itself contribute to the apparent fetal growth delay typical of this strain (Kulandavelu et al. 2006; Rennie et al. 2012). In addition, dysregulated cell death in the human placenta could be a mitigating factor in gestational diseases such as IUGR. Several studies have demonstrated higher rates of apoptosis in placental villi complicated by IUGR (Levy et al. 2002; Crocker et al. 2003; Longtine et al. 2012; Cali et al. 2013). Combined, these data support the notion that C57Bl/6 placentae are associated with a putative growth-restricted phenotype of C57Bl/6 fetuses.

In order to better understand the molecular mechanisms of cell death in the murine placenta, we examined the expression patterns of various well-known cell death-mediating proteins, including caspase-3. Interestingly, both ICR and C57Bl/6 placental lysates exhibited caspase-3 cleavage patterns that did not correlate with TUNEL staining. In addition, ICR placentas showed a significant increase in caspase-3 activity compared to C57Bl/6, which did not correlate with the lower overall rates of TUNEL-positive staining observed in ICR placentas.

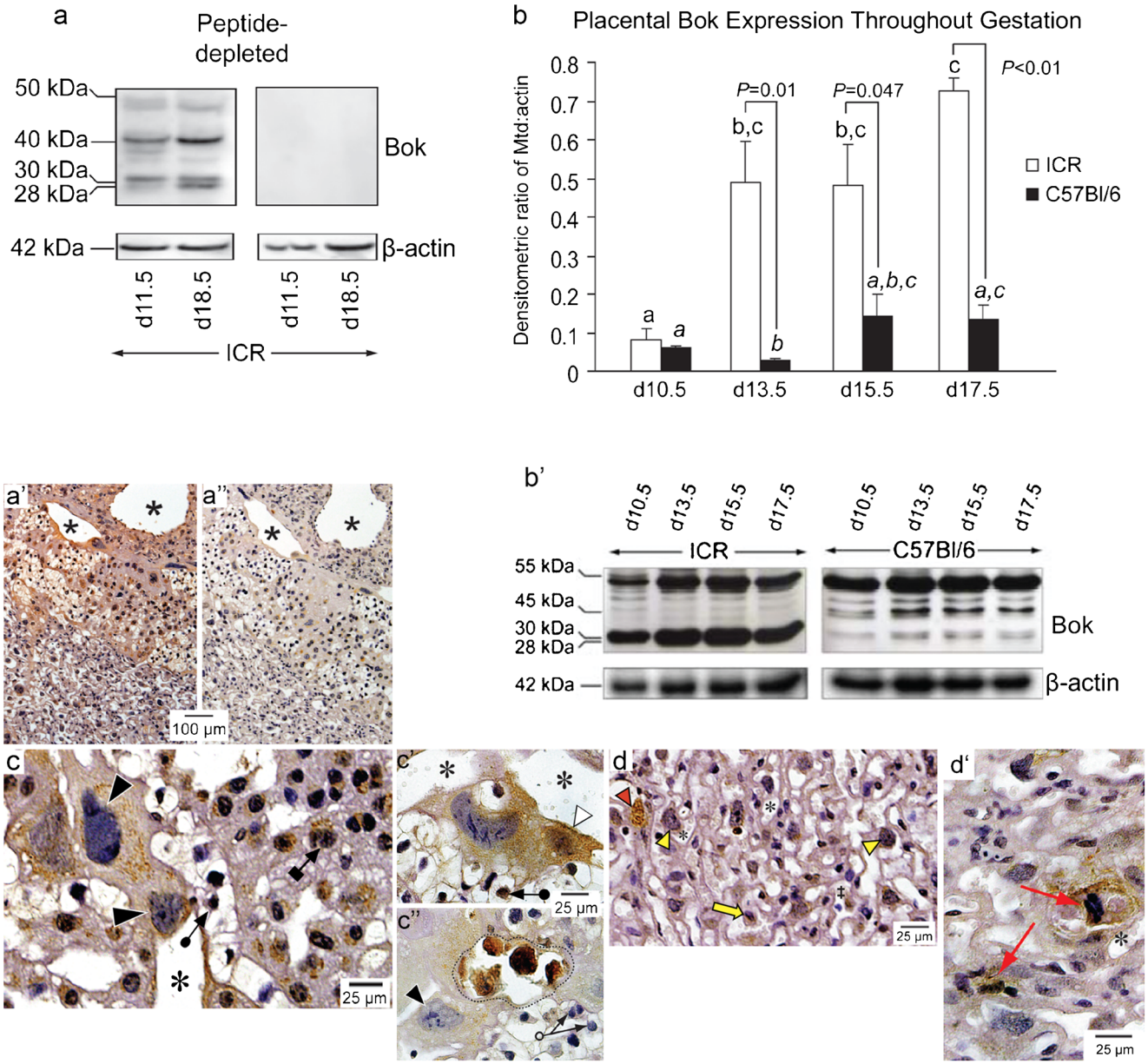

Fig. 7 Bok expression localizes to all regions of the mouse placenta and gradually increases throughout gestation. Representative immunoblot (**a**) and placental sections after probing with mock-depleted (**a'**) and peptide-depleted (**a"**) anti-Bok antibody, demonstrating specificity of the antibody. **b** Bok expression throughout gestation in placental lysates, as a densitometric ratio of Bok:β-actin after Western blotting. Bars represent average values ± SE and $n = 3$ for both ICR and C57Bl/6 placentae. **b'** Representative immunoblot of the Bok band(s) and the corresponding β-actin band. **c** Representative photomicrographs exhibiting Bok immunolocalization in the junctional zone. Within the junctional zone, healthy TGCs (filled arrowheads) and spongiotrophoblast cells (arrow with square end) exhibit lower levels of punctuate, perinuclear Bok expression. **c'** Early apoptotic TGCs (hollow arrowhead) display higher Bok expression, accompanied by translocation of this protein into the nucleus. **c"** Dotted line encircles a late apoptotic/necrotic TGC, exhibiting intense Bok staining of the debris. Also within the junctional zone are subsets of Bok-positive (arrows with closed-circle end) and Bok-negative (arrows with open-circle ends) trophoblast glycogen cells. **d** Representative photomicrographs exhibiting Bok immunolocalization in the labyrinth. Within the labyrinth, healthy sinusoidal TGCs (yellow arrowheads) express low levels of Bok, localized to the perinuclear region, while dead or dying sinusoidal TGCs (red arrowhead) demonstrate Bok reactivity throughout the cytoplasm and nucleus. Healthy ST cells (yellow arrow) express low levels of perinuclear Bok. **d'** Dead/dying ST cells (red arrows) exhibit more intense Bok staining, which was evident throughout the cell, including the nuclei. Fetal vessels are indicated by (‡) and asterisks (*) demarcate maternal blood spaces. Within the same strain over gestation, means with the same letter are not significantly different from each other (Tukey-Kramer test, $P < 0.05$). Values of significant statistical difference between ICR and C57Bl/6 placentae are shown with corresponding P value (Tukey-Kramer test)

These discrepancies could reflect alternative cell death pathways or non-apoptotic functions of caspase-3 in trophoblast. Indeed, several studies have highlighted the important role caspase enzymes play in regulating proliferation and

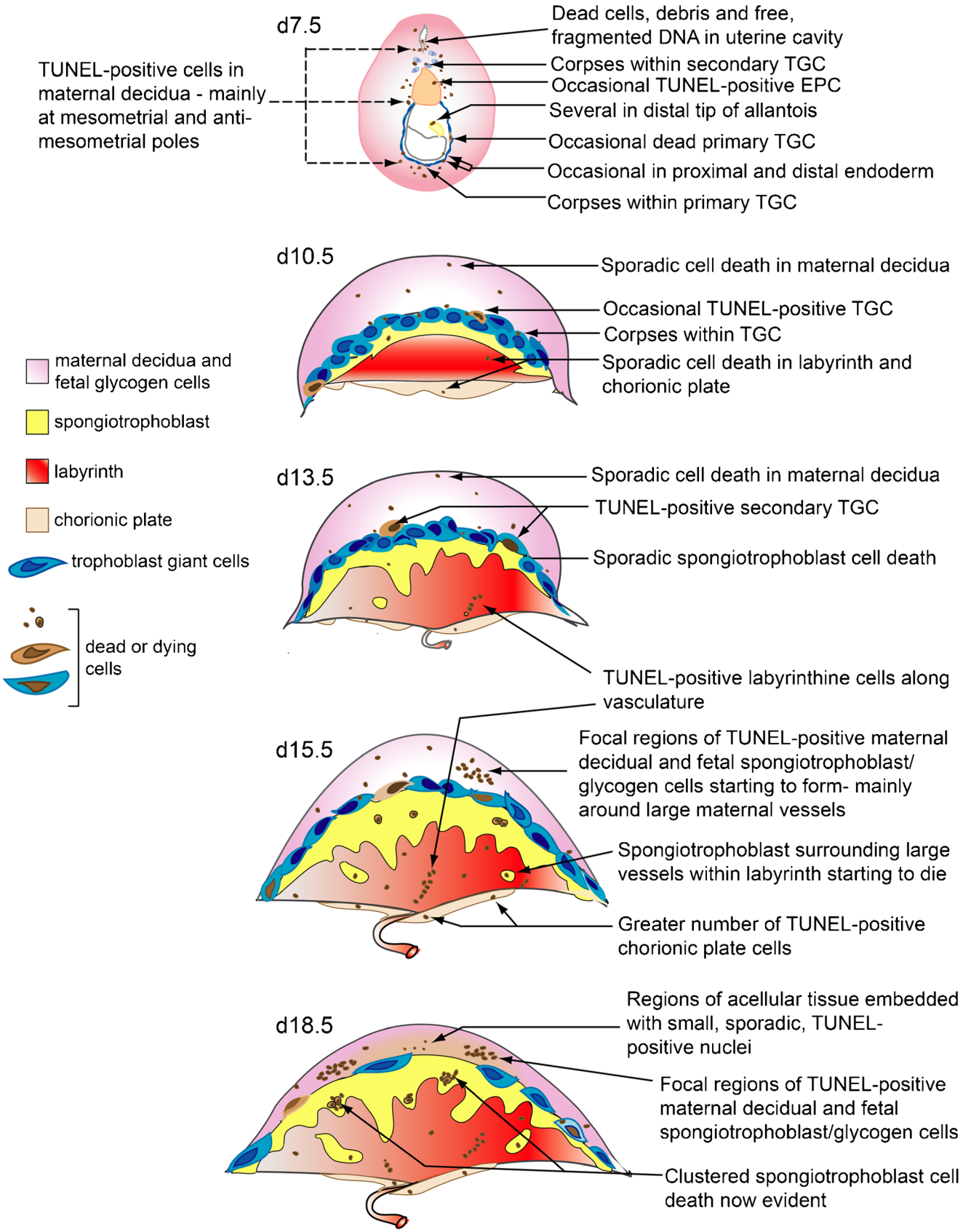

Fig. 8 Schematic representation of cell death patterns over development in the mouse placenta. Pictures reflect typical cell death patterns as revealed by TUNEL that were observed in transverse sections of ICR conceptuses and placentae at the time points examined in this study

differentiation of various cell types (Lamkanfi et al. 2007; Shalini et al. 2015). Notably, caspase-3 has been shown to promote differentiation of embryonic, muscle and hematopoietic stem cells (Fernando et al. 2002; Fujita et al. 2008; Janzen et al. 2008). It is also important to note that while TUNEL is an accepted method for measuring late stages of apoptosis, it can also detect other types of non-apoptotic cell death, such as necrosis or autolysis (Grasl-Kraupp et al. 1995). In addition, since molecular markers of apoptosis (i.e., cleaved caspase-3 and Parp-1) are transient and represent different stages of death, they rarely overlap with TUNEL. This has been previously observed in time-dependent analyses of cell death where both caspase-3 and/or Parp-1 activation preceded the detection of TUNEL (Sundquist et al. 2006; Namura et al. 2018).

Parp-1 is a known target of caspase-3 that has also been shown to be involved in alternative cell death pathways, including necrosis and autophagy (Rodríguez-Vargas et al. 2012; Sosna et al. 2014). Thus, examination of Parp-1 cleavage provided insight into possible alternative pathways of cell death throughout placentation. In placental lysates of both strains, we observed the presence of Parp-1 cleavage fragments at ~75 and 52 kDa but a complete absence of the canonical 89 and 25 kDa fragments, known to be a hallmark of caspase-mediated apoptosis (Lazebnik et al. 1994; Cali et al. 2013). Cells undergoing necrotic death have been reported to exhibit a different Parp-1 cleavage profile, yielding two major bands at 89 and 50 kDa (Shah et al. 1996). In addition, lysosomal cathepsins have been implicated in the production of a 72 and 55 kDa Parp-1 cleavage profile (Gobeil et al. 2001). Cell death triggered by the lysosomal pathway is not always necrotic in nature, as certain signals induce cathepsin release from lysosomes, leading to the activation of the apoptotic pathway (Chwieralski et al. 2006). Additionally, calpain, which is a Ca^{2+}-dependent non-lysosomal cysteine protease, has likewise been shown to produce 70 kDa (Boland and Campbell 2003) and 40 kDa (McGinnis et al. 1999) Parp-1 cleavage fragments. Our finding of parallel 75 kDa Parp-1 and cleaved caspase-3 expression levels in ICR placentae is in stark contrast to the data obtained in C57Bl/6 placentae, which demonstrated a peak in the 75 kDa Parp-1 cleavage product at d11.5 that remained relatively high throughout gestation. Interestingly, the pattern of 52 kDa Parp-1 expression differed significantly between the two strains and from their respective caspase-3 cleavage profiles. This suggests activation of different caspases or alternate Parp-1 processing pathways in C57Bl/6 and ICR placentae. Another possibility is that differing Parp-1 cleavage profiles between the two mouse strains may be a sign of alternate trophoblast differentiation, as both calpains and cathepsins are involved in regulating placental development and differentiation events (Dear and Boehm 1999; Varanou et al. 2006; Screen et al. 2008).

Bok, a pro-apoptotic member of the Bcl-2 family, has been shown to regulate trophoblast cell fate events (Soleymanlou et al. 2007; Ray et al. 2010). In addition, a human-specific, pro-apoptotic isoform of Bok has been associated with elevated trophoblast cell death in placentas from preeclamptic pregnancies (Soleymanlou et al. 2005). In the present study, we show that Bok is expressed in the murine placenta with the highest levels observed towards the end of pregnancy for both strains examined. Importantly, placental Bok expression during mid- to late-gestation was significantly higher in ICR placentas compared to C57Bl/6, which does not correlate with the comparatively lower rates of TUNEL-positive staining in the placentae of this strain. Such evidence may reflect non-apoptotic functions of Bok, such as regulating autophagy (Kalkat et al. 2013; Melland-Smith et al. 2015) or cell proliferation (Ray et al. 2010) and mitochondrial dynamics (Ausman et al. 2018). Although several studies have shown that overexpression of Bok in in vitro can induce cell death, the role and mechanism of Bok action is still debated. Surprisingly, initial analysis of Bok null mice ($Bok^{-/-}$) found that these mice display no developmental abnormalities, as mice are fertile and respond normally to apoptotic stimuli (Ke et al. 2012). Alternative or overlapping functions of Bok with its closely related Bcl-2 family members, Bax and Bak, may explain the lack of obvious phenotype. Both Bax and Bak respond to apoptotic stimuli by inducing mitochondrial outer membrane permeabilization (MOMP), which promotes caspase activation, eventually leading to cell death (Finucane et al. 1999). Unlike Bax and Bak, which are found at the mitochondria, Bok localizes primarily to the membranes of the endoplasmic reticulum (ER) and Golgi apparatus (Echeverry et al. 2013). Given its subcellular location, Bok has more recently been implicated in regulating ER stress-induced apoptosis. Initial reports did not find any evidence of ER stress-induced apoptosis in Bok-deficient cells (Echeverry et al. 2013); however, a later study reported that a lack of Bok did in fact result in failure to respond to ER stress (Carpio et al. 2015). It is important to note that while both groups demonstrated complete loss of Bok protein expression in their models, different segments of the Bok gene were altered and this may contribute to the contradictory results. Recently, triple knock-out (KO) $Bok^{-/-}/Bax^{-/-}/Bak^{-/-}$ mice were created, which displayed severe embryonic defects and earlier in utero deaths when compared to $Bax^{-/-}/Bak^{-/-}$ mice, indicating that Bok is functionally redundant with respect to Bak and Bax during embryonic development (Ke et al. 2018). While various developmental abnormalities in these triple KO embryos were observed, no examination of the placental phenotype in affected fetuses was reported.

The conflicting data for the function and mechanisms of Bok highlights the potential alternative roles it may play throughout development. It is also important to note that the role of Bok in determining cell fate may be cell type specific. For example, although commonly assumed to be pro-apoptotic, Bok has more recently been shown to play a protective role against apoptosis in neurons exposed to oxygen/glucose deprivation (D'Orsi et al. 2016). Finally, irrespective of the magnitude of expression, post-translational modifications or protein-protein interactions can also impact the functionality of this multidomain protein, as has been previously described for other members of the Bcl-2 family.

In conclusion, the patterns and rates of cell death in murine placentae change throughout gestation, with striking differences observed between ICR and C57Bl/6 strains. These differences may be important to consider when analyzing and interpreting various murine models of placental disease. Overall, cell death patterns in both ICR and C57Bl/6 placentae across gestation are similar to those seen in human placentae, with increased cell death occurring towards term. It is evident that cell death is involved in shaping the vasculature of the murine labyrinth and in preparing the maternal and fetal compartments of the placenta for impending separation at parturition. Establishing the molecular pathways functioning in cell death during murine placentation will provide a useful framework to further investigations into the dysregulation of this pathway in human gestational diseases.

Funding This work was supported by research grants from the SickKids Foundation and NSERC (RGPIN-04497) to AJ and Canadian Institute of Health Research (MOP-89813) awarded to IC. During these studies, JD was funded by a Doctoral Research Award from the National Sciences and Engineering Research Council, JR was funded by CIHR DRA scholarship and Genesis foundation OGS program and IR was supported by LTRI-OSOTF program.

Compliance with ethical standards

Conflict of interest The authors declare that they have no conflict of interest.

Ethical approval All mouse experiments were performed in accordance with the Canadian Council on Animal Care (CCAC) guidelines for Use of Animals in Research and Laboratory Animal Care under protocols approved by animal care committees at Mount Sinai Hospital or the Toronto Centre for Phenogenomics.

Informed consent Not applicable.

References

Ausman J, Abbade J, Ermini L, Farrell A, Tagliaferro A, Post M, Caniggia I (2018) Ceramide-induced BOK promotes mitochondrial fission in preeclampsia. Cell Death Dis 9:298

Bailey LJ, Alahari S, Tagliaferro A, Post M, Caniggia I (2017) Augmented trophoblast cell death in preeclampsia can proceed via ceramide-mediated necroptosis. Cell Death Dis 8:1–14

Boland B, Campbell V (2003) beta-Amyloid (1-40)-induced apoptosis of cultured cortical neurones involves calpain-mediated cleavage of poly-ADP-ribose polymerase. Neurobiol Aging 24:179–186

Bouillot S, Rampon C, Tillet E, Huber P (2006) Tracing the glycogen cells with protocadherin 12 during mouse placenta development. Placenta 27:882–888

Cali U, Cavkaytar S, Sirvan L, Danisman N (2013) Placental apoptosis in preeclampsia, intrauterine growth retardation, and HELLP syndrome: an immunohistochemical study with caspase-3 and bcl-2. Clin Exp Obstet Gynecol 40:45–48

Carpio MA, Michaud M, Zhou W, Fisher JK, Walensky LD, Katz SG (2015) BCL-2 family member BOK promotes apoptosis in response to endoplasmic reticulum stress. Proc Natl Acad Sci 112:7201–7206

Chwieralski CE, Welte T, Bühling F (2006) Cathepsin-regulated apoptosis. Apoptosis 11:143–149

Coan PM, Conroy N, Burton GJ, Ferguson-Smith AC (2006) Origin and characteristics of glycogen cells in the developing murine placenta. Dev Dyn 235:3280–3294

Cox B, Kotlyar M, Evangelou AI, Ignatchenko V, Ignatchenko A, Whiteley K, Jurisica I, Adamson SL, Rossant J, Kislinger T (2009) Comparative systems biology of human and mouse as a tool to guide the modeling of human placental pathology. Mol Syst Biol 5:1–15

Crocker IP, Cooper S, Ong SC, Baker PN (2003) Differences in apoptotic susceptibility of cytotrophoblasts and syncytiotrophoblasts in normal pregnancy to those complicated with preeclampsia and intrauterine growth restriction. Am J Pathol 162:637–643

Cross JC, Hemberger M, Lu Y, Nozaki T, Whiteley K, Masutani M, Adamson SL (2002) Trophoblast functions, angiogenesis and remodeling of the maternal vasculature in the placenta. Mol Cell Endocrinol 187:207–212

D'Orsi B, Engel T, Pfeiffer S, Nandi S, Kaufmann T, Henshall DC, Prehn JHM (2016) Bok is not pro-apoptotic but suppresses poly ADP-ribose polymerase-dependent cell death pathways and protects against excitotoxic and seizure-induced neuronal injury. J Neurosci 36:4564–4578

Dear TN, Boehm T (1999) Diverse mRNA expression patterns of the mouse calpain genes Capn5, Capn6 and Capn11 during development. Mech Dev 89:201–209

Detmar J, Rabaglino T, Taniuchi Y, Oh J, Acton BM, Benito A, Nunez G, Jurisicova A (2006) Embryonic loss due to exposure to polycyclic aromatic hydrocarbons is mediated by Bax. Apoptosis 11:1413–1425

Detmar J, Rennie MY, Whiteley KJ, Qu D, Taniuchi Y, Shang X, Casper RF, Adamson SL, Sled JG, Jurisicova A, Detmar J, My R, Kj W, Qu D, Taniuchi Y, Rf C, Sl A, Jg S, J a F (2008) Fetal growth restriction triggered by polycyclic aromatic hydrocarbons is associated with altered placental vasculature and AhR -dependent changes in cell death. Am Physiol Soc 5:519–530

Dimmeler S, Zeiher AM (2000) Endothelial cell apoptosis in angiogenesis and vessel regression. Circ Res 87:434–439

Doetschman T, Parkitna JR, Engblom D, Tessarollo L, Palko ME, Akagi K, Coppola V, Ku R, Wurst W, Lee S, Wang W, Liu P (2009) Gene knockout protocols. Gene 530:15–27

Echeverry N, Bachmann D, Ke F, Strasser A, Simon HU, Kaufmann T (2013) Intracellular localization of the BCL-2 family member BOK and functional implications. Cell Death Differ 20:785–799

Fernando P, Kelly JF, Balazsi K, Slack RS, Megeney LA (2002) Caspase 3 activity is required for skeletal muscle differentiation. Proc Natl Acad Sci U S A 99:11025–11030

Finucane DM, Bossy-wetzel E, Waterhouse NJ, Cotter TG, Green DR (1999) Bax-induced caspase activation and apoptosis via

cytochrome c release from mitochondria is inhibitable by Bcl-xL. J Biol Chem 274:2225–2233
Fuchs Y, Steller H (2011) Programmed cell death in animal development and disease. Cell 147:742–758
Fujita J, Crane AM, Souza MK, Dejosez M, Kyba M, Flavell RA, Thomson JA, Zwaka TP (2008) Caspase activity mediates the differentiation of embryonic stem cells. Cell Stem Cell 2:595–601
Georgiades P, Fergyson-Smith AC, Burton GJ (2002) Comparative developmental anatomy of the murine and human definitive placentae. Placenta 23:3–19
Gobeil S, Boucher CC, Nadeau D, Poirier GG (2001) Characterization of the necrotic cleavage of poly (ADP-ribose) polymerase (PARP-1): implication of lysosomal proteases. Cell Death Differ 8:588–594
Gong J-S, Kim GJ (2014) The role of autophagy in the placenta as a regulator of cell death. Clin Exp Reprod Med 41:97–107
Grasl-Kraupp B, Ruttkay-Nedecky B, Koudelka H, Bukowska K, Bursch W, Schulte-Hermann R (1995) In situ detection of fragmented DNA (tunel assay) fails to discriminate among apoptosis, necrosis, and autolytic cell death: a cautionary note. Hepatology 21:1465–1468
Hu D, Cross JC (2010) Development and function of trophoblast giant cells in the rodent. placenta. 354:341–354
Hung TH, Chen SF, Lo LM, Li MJ, Yeh YL, Hsieh TT (2012) Increased autophagy in placentas of intrauterine growth-restricted pregnancies. PLoS One 7:e40957
Huppertz B, Kingdom JCP (2004) Apoptosis in the trophoblast–role of apoptosis in placental morphogenesis. J Soc Gynecol Investig 11: 353–362
Huppertz B, Frank HG, Kingdom JCP, Reister F, Kaufmann P (1998) Villous cytotrophoblast regulation of the syncytial apoptotic cascade in the human placenta. Histochem Cell Biol 110:495–508
Janzen V, Fleming HE, Riedt T, Karlsson G, Riese MJ, Lo Celso C, Reynolds G, Milne CD, Paige CJ, Karlsson S, Woo M, Scadden DT (2008) Hematopoietic stem cell responsiveness to exogenous signals is limited by caspase-3. Cell Stem Cell 2:584–594
Jurisicova A, Detmar J, Caniggia I (2005) Molecular mechanisms of trophoblast survival: from implantation to birth. Birth Defects Res Part C - Embryo Today Rev 75:262–280
Kalkat M, Garcia J, Ebrahimi J, Melland-Smith M, Todros T, Post M, Caniggia I (2013) Placental autophagy regulation by the BOK-MCL1 rheostat. Autophagy 9:2140–2153
Ke F, Voss A, Kerr JB, O'Reilly LA, Tai L, Echeverry N, Bouillet P, Strasser A, Kaufmann T (2012) BCL-2 family member BOK is widely expressed but its loss has only minimal impact in mice. Cell Death Differ 19:915–925
Ke FFS, Vanyai HK, Cowan AD, Delbridge ARD, Whitehead L, Grabow S, Czabotar PE, Voss AK, Strasser A (2018) Embryogenesis and adult life in the absence of intrinsic apoptosis effectors BAX, BAK, and BOK. Cell 173:1217–1230.e17
Kroemer G, Galluzzi L, Vandenabeele P, Abrams J, Alnemri ES, Baehrecke EH, Blagosklonny MV, El-Deiry WS, Golstein P, Green DR, Hengartner M, Knight RA, Kumar S, Lipton SA, Malorni W, Nuñez G, Peter ME, Tschopp J, Yuan J, Piacentini M, Zhivotovsky B, Melino G (2009) Classification of cell death: recommendations of the nomenclature committee on cell death 2009. Cell Death Differ 16:3–11
Kulandavelu S, Qu D, Sunn N, Mu J, Rennie MY, Whiteley KJ, Walls JR, Bock NA, Sun JCH, Covelli A, Sled JG, Adamson SL (2006) Embryonic and neonatal phenotyping of genetically engineered mice. ILAR J 47:103–117
Kyathanahalli C, Marks J, Nye K, Lao B, Albrecht ED, Aberdeen GW, Nathanielsz PW, Jeyasuria P, Condon JC (2013) Cross-species withdrawal of MCL1 facilitates postpartum uterine involution in both the mouse and baboon. Endocrinology 154:4873–4884
Lamkanfi M, Festjens N, Declercq W, Vanden Berghe T, Vandenabeele P (2007) Caspases in cell survival, proliferation and differentiation. Cell Death Differ 14:44–55
Lazebnik YA, Kaufmann SH, Desnoyers S, Poirier GG, Earnshaw WC (1994) Cleavage of poly (ADP-ribose) polymerase by a proteinase with properties like ICE. Nature 371:346–347
Levy R, Smith SD, Yusuf K, Huettner PC, Kraus FT, Sadovsky Y, Nelson DM (2002) Trophoblast apoptosis from pregnancies complicated by fetal growth restriction is associated with enhanced p53 expression. Am J Obs Gynecol 186:1056–1061
Linder CC (2006) Genetic variables that influence phenotype. ILAR J 47: 132–140
Longtine MS, Chen B, Odibo AO, Zhong Y, Nelson DM (2012) Villous trophoblast apoptosis is elevated and restricted to cytotrophoblasts in pregnancies complicated by preeclampsia, IUGR, or preeclampsia with IUGR. Placenta 33:352–359
McGinnis KM, Gnegy ME, Park YH, Mukerjee N, Wang KK (1999) Procaspase-3 and poly (ADP) ribose polymerase (PARP) are calpain substrates. Biochem Biophys Res Commun 263:94–99
Melland-Smith M, Ermini L, Chauvin S, Craig-Barnes H, Tagliaferro A, Todros T, Post M, Caniggia I (2015) Disruption of sphingolipid metabolism augments ceramide-induced autophagy in preeclampsia. Autophagy 11:653–669
Nadhan R, Vaman JV, Nirmala C, Kumar Sengodan S, Krishnakumar Hemalatha S, Rajan A, Varghese GR, RL N, BV AK, Thankappan R, Srinivas P (2017) Insights into dovetailing GTD and cancers. Crit Rev Oncol Hematol 114:77–90
Namura S, Zhu J, Fink K, Endres M, Srinivasan A, Tomaselli KJ, Yuan J, Moskowitz MA (2018) Activation and cleavage of caspase-3 in apoptosis induced by experimental cerebral ischemia. J Neurosci 18:3659–3668
Penaloza C, Lin L, Lockshin RA, Zakeri Z (2006) Cell death in development: shaping the embryo. Histochem Cell Biol 126:149–158
Ray JE, Garcia J, Jurisicova A, Caniggia I (2010) Mtd/Bok takes a swing: proapoptotic Mtd/Bok regulates trophoblast cell proliferation during human placental development and in preeclampsia. Cell Death Differ 17:846–859
Rennie MY, Whiteley KJ, Jurisicova A, Detmar J, Adamson SL, Sled JG (2012) Expansion of the fetoplacental vasculature in late gestation is strain dependent in mice. Am J Physiol Circ Physiol 302:H1261–H1273
Rodríguez-Vargas JM, Ruiz-Magãa MJ, Ruiz-Ruiz C, Majuelos-Melguizo J, Peralta-Leal A, Rodríguez MI, Muñoz-Gámez JA, De Almodóvar MR, Siles E, Rivas AL, Jäättela M, Oliver FJ (2012) ROS-induced DNA damage and PARP-1 are required for optimal induction of starvation-induced autophagy. Cell Res 22:1181–1198
Rossant J, Cross JC (2001) Placental development: lessons from mouse mutants. Nat Rev Genet 2:538–548
Screen M, Dean W, Cross JC, Hemberger M (2008) Cathepsin proteases have distinct roles in trophoblast function and vascular remodelling. Development 135:3311–3320
Shah GM, Shah RG, Poirier GG (1996) Different cleavage pattern for poly (ADP-ribose) polymerase during necrosis and apoptosis in HL-60 cells (1 , 2). These two forms of cell death are generally characterized by visualizing the disruption (1 , 3). Since proteases play a crucial role in. Biochem Biophys Res Commun 844:838–844
Shalini S, Dorstyn L, Dawar S, Kumar S (2015) Old, new and emerging functions of caspases. Cell Death Differ 22:526–539
Sharp AN, Heazell AEP, Crocker IP, Mor G (2010) Placental apoptosis in health and disease. Am J Reprod Immunol 64:159–169
Smith SC, Baker PN, Symonds EM (1997) Placental apoptosis in normal human pregnancy. Am J Obstet Gynecol 177:57–65
Smith SC, Leung TN, To KF, Baker PN (2000) Apoptosis is a rare event in first-trimester placental tissue. Am J Obstet Gynecol 183:697–699
Soleymanlou N, Wu Y, Wang JX, Todros T, Ietta F, Jurisicova A, Post M, Caniggia I (2005) A novel Mtd splice isoform is responsible for trophoblast cell death in pre-eclampsia. Cell Death Differ 12:441–452

Soleymanlou N, Jurisicova A, Wu Y, Chijiiwa M, Ray JE, Detmar J, Todros T, Zamudio S, Post M, Caniggia I (2007) Hypoxic switch in mitochondrial myeloid cell leukemia factor-1/Mtd apoptotic rheostat contributes to human trophoblast cell death in preeclampsia. Am J Pathol 171:496–506

Soncin F, Khater M, To C, Pizzo D, Farah O, Wakeland A, Arul Nambi Rajan K, Nelson KK, Chang C-W, Moretto-Zita M, Natale DR, Laurent LC, Parast MM (2018) Comparative analysis of mouse and human placentae across gestation reveals species-specific regulators of placental development. Development 145:dev156273

Sosna J, Voigt S, Mathieu S, Lange A, Thon L, Davarnia P, Herdegen T, Linkermann A, Rittger A, Chan FKM, Kabelitz D, Schutze S, Adam D (2014) TNF-induced necroptosis and PARP-1-mediated necrosis represent distinct routes to programmed necrotic cell death. Cell Mol Life Sci 71:331–348

Sundquist T, Moravec R, Niles A, O'Brien M, Riss T, Corporation P (2006) Timing your apoptosis assays. Cell Notes 16:18–21

Tertemiz F (2005) Apoptosis contributes to vascular lumen formation and vascular branching in human placental vasculogenesis. Biol Reprod 72:727–735

Varanou A, Withington SL, Lakasing L, Williamson C, Burton GJ, Hemberger M (2006) The importance of cysteine cathepsin proteases for placental development. J Mol Med 84:305–317